# Measurement of the $p\overline{p} \to W\gamma + X$ cross section at $\sqrt{s} = 1.96$ TeV and $WW\gamma$ anomalous coupling limits

arXiv:hep-ex/0503048v1 28 Mar 2005

V.M. Abazov,[35] B. Abbott,[72] M. Abolins,[63] B.S. Acharya,[29] M. Adams,[50] T. Adams,[48] M. Agelou,[18] J.-L. Agram,[19] S.H. Ahn,[31] M. Ahsan,[57] G.D. Alexeev,[35] G. Alkhazov,[39] A. Alton,[62] G. Alverson,[61] G.A. Alves,[2] M. Anastasoaie,[34] T. Andeen,[52] S. Anderson,[44] B. Andrieu,[17] Y. Arnoud,[14] A. Askew,[48] B. Åsman,[40] A.C.S. Assis Jesus,[3] O. Atramentov,[55] C. Autermann,[21] C. Avila,[8] F. Badaud,[13] A. Baden,[59] B. Baldin,[49] P.W. Balm,[33] S. Banerjee,[29] E. Barberis,[61] P. Bargassa,[76] P. Baringer,[56] C. Barnes,[42] J. Barreto,[2] J.F. Bartlett,[49] U. Bassler,[17] D. Bauer,[53] A. Bean,[56] S. Beauceron,[17] M. Begel,[68] A. Bellavance,[65] S.B. Beri,[27] G. Bernardi,[17] R. Bernhard,[49,*] I. Bertram,[41] M. Besançon,[18] R. Beuselinck,[42] V.A. Bezzubov,[38] P.C. Bhat,[49] V. Bhatnagar,[27] M. Binder,[25] C. Biscarat,[41] K.M. Black,[60] I. Blackler,[42] G. Blazey,[51] F. Blekman,[33] S. Blessing,[48] D. Bloch,[19] U. Blumenschein,[23] A. Boehnlein,[49] O. Boeriu,[54] T.A. Bolton,[57] F. Borcherding,[49] G. Borissov,[41] K. Bos,[33] T. Bose,[67] A. Brandt,[74] R. Brock,[63] G. Brooijmans,[67] A. Bross,[49] N.J. Buchanan,[48] D. Buchholz,[52] M. Buehler,[50] V. Buescher,[23] S. Burdin,[49] T.H. Burnett,[78] E. Busato,[17] C.P. Buszello,[42] J.M. Butler,[60] J. Bystricky,[18] S. Caron,[33] W. Carvalho,[3] B.C.K. Casey,[73] N.M. Cason,[54] H. Castilla-Valdez,[32] S. Chakrabarti,[29] D. Chakraborty,[51] K.M. Chan,[68] A. Chandra,[29] D. Chapin,[73] F. Charles,[19] E. Cheu,[44] D.K. Cho,[60] S. Choi,[47] B. Choudhary,[28] T. Christiansen,[25] L. Christofek,[56] D. Claes,[65] B. Clément,[19] C. Clément,[40] Y. Coadou,[5] M. Cooke,[76] W.E. Cooper,[49] D. Coppage,[56] M. Corcoran,[76] A. Cothenet,[15] M.-C. Cousinou,[15] B. Cox,[43] S. Crépé-Renaudin,[14] D. Cutts,[73] H. da Motta,[2] B. Davies,[41] G. Davies,[42] G.A. Davis,[52] K. De,[74] P. de Jong,[33] S.J. de Jong,[34] E. De La Cruz-Burelo,[32] C. De Oliveira Martins,[3] S. Dean,[43] J.D. Degenhardt,[62] F. Déliot,[18] M. Demarteau,[49] R. Demina,[68] P. Demine,[18] D. Denisov,[49] S.P. Denisov,[38] S. Desai,[69] H.T. Diehl,[49] M. Diesburg,[49] M. Doidge,[41] H. Dong,[69] S. Doulas,[61] L.V. Dudko,[37] L. Duflot,[16] S.R. Dugad,[29] A. Duperrin,[15] J. Dyer,[63] A. Dyshkant,[51] M. Eads,[51] D. Edmunds,[63] T. Edwards,[43] J. Ellison,[47] J. Elmsheuser,[25] V.D. Elvira,[49] S. Eno,[59] P. Ermolov,[37] O.V. Eroshin,[38] J. Estrada,[49] H. Evans,[67] A. Evdokimov,[36] V.N. Evdokimov,[38] J. Fast,[49] S.N. Fatakia,[60] L. Feligioni,[60] T. Ferbel,[68] F. Fiedler,[25] F. Filthaut,[34] W. Fisher,[66] H.E. Fisk,[49] I. Fleck,[23] M. Fortner,[51] H. Fox,[23] S. Fu,[49] S. Fuess,[49] T. Gadfort,[78] C.F. Galea,[34] E. Gallas,[49] E. Galyaev,[54] C. Garcia,[68] A. Garcia-Bellido,[78] J. Gardner,[56] V. Gavrilov,[36] P. Gay,[13] D. Gelé,[19] R. Gelhaus,[47] K. Genser,[49] C.E. Gerber,[50] Y. Gershtein,[48] D. Gillberg,[5] G. Ginther,[68] T. Golling,[22] N. Gollub,[40] B. Gómez,[8] K. Gounder,[49] A. Goussiou,[54] P.D. Grannis,[69] S. Greder,[3] H. Greenlee,[49] Z.D. Greenwood,[58] E.M. Gregores,[4] Ph. Gris,[13] J.-F. Grivaz,[16] L. Groer,[67] S. Grünendahl,[49] M.W. Grünewald,[30] S.N. Gurzhiev,[38] G. Gutierrez,[49] P. Gutierrez,[72] A. Haas,[67] N.J. Hadley,[59] S. Hagopian,[48] I. Hall,[72] R.E. Hall,[46] C. Han,[62] L. Han,[7] K. Hanagaki,[49] K. Harder,[57] A. Harel,[26] R. Harrington,[61] J.M. Hauptman,[55] R. Hauser,[63] J. Hays,[52] T. Hebbeker,[21] D. Hedin,[51] J.M. Heinmiller,[50] A.P. Heinson,[47] U. Heintz,[60] C. Hensel,[56] G. Hesketh,[61] M.D. Hildreth,[54] R. Hirosky,[77] J.D. Hobbs,[69] B. Hoeneisen,[12] M. Hohlfeld,[24] S.J. Hong,[31] R. Hooper,[73] P. Houben,[33] Y. Hu,[69] J. Huang,[53] V. Hynek,[9] I. Iashvili,[47] R. Illingworth,[49] A.S. Ito,[49] S. Jabeen,[56] M. Jaffré,[16] S. Jain,[72] V. Jain,[70] K. Jakobs,[23] A. Jenkins,[42] R. Jesik,[42] K. Johns,[44] M. Johnson,[49] A. Jonckheere,[49] P. Jonsson,[42] A. Juste,[49] D. Käfer,[21] S. Kahn,[70] E. Kajfasz,[15] A.M. Kalinin,[35] J. Kalk,[63] D. Karmanov,[37] J. Kasper,[60] D. Kau,[48] R. Kaur,[27] R. Kehoe,[75] S. Kermiche,[15] S. Kesisoglou,[73] A. Khanov,[68] A. Kharchilava,[54] Y.M. Kharzheev,[35] H. Kim,[74] T.J. Kim,[31] B. Klima,[49] J.M. Kohli,[27] M. Kopal,[72] V.M. Korablev,[38] J. Kotcher,[70] B. Kothari,[67] A. Koubarovsky,[37] A.V. Kozelov,[38] J. Kozminski,[63] A. Kryemadhi,[77] S. Krzywdzinski,[49] Y. Kulik,[49] A. Kumar,[28] S. Kunori,[59] A. Kupco,[11] T. Kurča,[20] J. Kvita,[9] S. Lager,[40] N. Lahrichi,[18] G. Landsberg,[73] J. Lazoflores,[48] A.-C. Le Bihan,[19] P. Lebrun,[20] W.M. Lee,[48] A. Leflat,[37] F. Lehner,[49,*] C. Leonidopoulos,[67] J. Leveque,[44] P. Lewis,[42] J. Li,[74] Q.Z. Li,[49] J.G.R. Lima,[51] D. Lincoln,[49] S.L. Linn,[48] J. Linnemann,[63] V.V. Lipaev,[38] R. Lipton,[49] L. Lobo,[42] A. Lobodenko,[39] M. Lokajicek,[11] A. Lounis,[19] P. Love,[41] H.J. Lubatti,[78] L. Lueking,[49] M. Lynker,[54] A.L. Lyon,[49] A.K.A. Maciel,[51] R.J. Madaras,[45] P. Mättig,[26] C. Magass,[21] A. Magerkurth,[62] A.-M. Magnan,[14] N. Makovec,[16] P.K. Mal,[29] H.B. Malbouisson,[3] S. Malik,[58] V.L. Malyshev,[35] H.S. Mao,[6] Y. Maravin,[49] M. Martens,[49] S.E.K. Mattingly,[73] A.A. Mayorov,[38] R. McCarthy,[69] R. McCroskey,[44] D. Meder,[24] H.L. Melanson,[49] A. Melnitchouk,[64] A. Mendes,[15] M. Merkin,[37] K.W. Merritt,[49] A. Meyer,[21] J. Meyer,[22] M. Michaut,[18] H. Miettinen,[76] J. Mitrevski,[67] J. Molina,[3] N.K. Mondal,[29] R.W. Moore,[5] G.S. Muanza,[20] M. Mulders,[49] Y.D. Mutaf,[69] E. Nagy,[15] M. Narain,[60] N.A. Naumann,[34] H.A. Neal,[62] J.P. Negret,[8] S. Nelson,[48] P. Neustroev,[39] C. Noeding,[23] A. Nomerotski,[49] S.F. Novaes,[4] T. Nunnemann,[25] E. Nurse,[43] V. O'Dell,[49]

D.C. O'Neil,[5] V. Oguri,[3] N. Oliveira,[3] N. Oshima,[49] G.J. Otero y Garzón,[50] P. Padley,[76] N. Parashar,[58] S.K. Park,[31]
J. Parsons,[67] R. Partridge,[73] N. Parua,[69] A. Patwa,[70] G. Pawloski,[76] P.M. Perea,[47] E. Perez,[18] P. Pétroff,[16]
M. Petteni,[42] R. Piegaia,[1] M.-A. Pleier,[68] P.L.M. Podesta-Lerma,[32] V.M. Podstavkov,[49] Y. Pogorelov,[54]
B.G. Pope,[63] W.L. Prado da Silva,[3] H.B. Prosper,[48] S. Protopopescu,[70] J. Qian,[62] A. Quadt,[22] B. Quinn,[64]
K.J. Rani,[29] K. Ranjan,[28] P.A. Rapidis,[49] P.N. Ratoff,[41] S. Reucroft,[61] M. Rijssenbeek,[69] I. Ripp-Baudot,[19]
F. Rizatdinova,[57] S. Robinson,[42] R.F. Rodrigues,[3] C. Royon,[18] P. Rubinov,[49] R. Ruchti,[54] V.I. Rud,[37] G. Sajot,[14]
A. Sánchez-Hernández,[32] M.P. Sanders,[59] A. Santoro,[3] G. Savage,[49] L. Sawyer,[58] T. Scanlon,[42] D. Schaile,[25]
R.D. Schamberger,[69] H. Schellman,[52] P. Schieferdecker,[25] C. Schmitt,[26] C. Schwanenberger,[22] A. Schwartzman,[66]
R. Schwienhorst,[63] S. Sengupta,[48] H. Severini,[72] E. Shabalina,[50] M. Shamim,[57] V. Shary,[18] A.A. Shchukin,[38]
W.D. Shephard,[54] R.K. Shivpuri,[28] D. Shpakov,[61] R.A. Sidwell,[57] V. Simak,[10] V. Sirotenko,[49] P. Skubic,[72]
P. Slattery,[68] R.P. Smith,[49] K. Smolek,[10] G.R. Snow,[65] J. Snow,[71] S. Snyder,[70] S. Söldner-Rembold,[43] X. Song,[51]
L. Sonnenschein,[17] A. Sopczak,[41] M. Sosebee,[74] K. Soustruznik,[9] M. Souza,[2] B. Spurlock,[74] N.R. Stanton,[57]
J. Stark,[14] J. Steele,[58] K. Stevenson,[53] V. Stolin,[36] A. Stone,[50] D.A. Stoyanova,[38] J. Strandberg,[40] M.A. Strang,[74]
M. Strauss,[72] R. Ströhmer,[25] D. Strom,[52] M. Strovink,[45] L. Stutte,[49] S. Sumowidagdo,[48] A. Sznajder,[3]
M. Talby,[15] P. Tamburello,[44] W. Taylor,[5] P. Telford,[43] J. Temple,[44] M. Tomoto,[49] T. Toole,[59] J. Torborg,[54]
S. Towers,[69] T. Trefzger,[24] S. Trincaz-Duvoid,[17] B. Tuchming,[18] C. Tully,[66] A.S. Turcot,[43] P.M. Tuts,[67]
L. Uvarov,[39] S. Uvarov,[39] S. Uzunyan,[51] B. Vachon,[5] R. Van Kooten,[53] W.M. van Leeuwen,[33] N. Varelas,[50]
E.W. Varnes,[44] A. Vartapetian,[74] I.A. Vasilyev,[38] M. Vaupel,[26] P. Verdier,[20] L.S. Vertogradov,[35] M. Verzocchi,[59]
F. Villeneuve-Seguier,[42] J.-R. Vlimant,[17] E. Von Toerne,[57] M. Vreeswijk,[33] T. Vu Anh,[16] H.D. Wahl,[48] L. Wang,[59]
J. Warchol,[54] G. Watts,[78] M. Wayne,[54] M. Weber,[49] H. Weerts,[63] M. Wegner,[21] N. Wermes,[22] A. White,[74]
V. White,[49] D. Wicke,[49] D.A. Wijngaarden,[34] G.W. Wilson,[56] S.J. Wimpenny,[47] J. Wittlin,[60] M. Wobisch,[49]
J. Womersley,[49] D.R. Wood,[61] T.R. Wyatt,[43] Q. Xu,[62] N. Xuan,[54] S. Yacoob,[52] R. Yamada,[49] M. Yan,[59]
T. Yasuda,[49] Y.A. Yatsunenko,[35] Y. Yen,[26] K. Yip,[70] H.D. Yoo,[73] S.W. Youn,[52] J. Yu,[74] A. Yurkewicz,[69]
A. Zabi,[16] A. Zatserklyaniy,[51] M. Zdrazil,[69] C. Zeitnitz,[24] D. Zhang,[49] X. Zhang,[72] T. Zhao,[78] Z. Zhao,[62]
B. Zhou,[62] J. Zhu,[69] M. Zielinski,[68] D. Zieminska,[53] A. Zieminski,[53] R. Zitoun,[69] V. Zutshi,[51] and E.G. Zverev[37]
(DØ Collaboration)
[1]*Universidad de Buenos Aires, Buenos Aires, Argentina*
[2]*LAFEX, Centro Brasileiro de Pesquisas Físicas, Rio de Janeiro, Brazil*
[3]*Universidade do Estado do Rio de Janeiro, Rio de Janeiro, Brazil*
[4]*Instituto de Física Teórica, Universidade Estadual Paulista, São Paulo, Brazil*
[5]*University of Alberta, Edmonton, Alberta, Canada, Simon Fraser University, Burnaby, British Columbia, Canada,*
*York University, Toronto, Ontario, Canada, and McGill University, Montreal, Quebec, Canada*
[6]*Institute of High Energy Physics, Beijing, People's Republic of China*
[7]*University of Science and Technology of China, Hefei, People's Republic of China*
[8]*Universidad de los Andes, Bogotá, Colombia*
[9]*Center for Particle Physics, Charles University, Prague, Czech Republic*
[10]*Czech Technical University, Prague, Czech Republic*
[11]*Institute of Physics, Academy of Sciences, Center for Particle Physics, Prague, Czech Republic*
[12]*Universidad San Francisco de Quito, Quito, Ecuador*
[13]*Laboratoire de Physique Corpusculaire, IN2P3-CNRS, Université Blaise Pascal, Clermont-Ferrand, France*
[14]*Laboratoire de Physique Subatomique et de Cosmologie, IN2P3-CNRS, Universite de Grenoble 1, Grenoble, France*
[15]*CPPM, IN2P3-CNRS, Université de la Méditerranée, Marseille, France*
[16]*Laboratoire de l'Accélérateur Linéaire, IN2P3-CNRS, Orsay, France*
[17]*LPNHE, IN2P3-CNRS, Universités Paris VI and VII, Paris, France*
[18]*DAPNIA/Service de Physique des Particules, CEA, Saclay, France*
[19]*IReS, IN2P3-CNRS, Université Louis Pasteur, Strasbourg, France, and Université de Haute Alsace, Mulhouse, France*
[20]*Institut de Physique Nucléaire de Lyon, IN2P3-CNRS, Université Claude Bernard, Villeurbanne, France*
[21]*III. Physikalisches Institut A, RWTH Aachen, Aachen, Germany*
[22]*Physikalisches Institut, Universität Bonn, Bonn, Germany*
[23]*Physikalisches Institut, Universität Freiburg, Freiburg, Germany*
[24]*Institut für Physik, Universität Mainz, Mainz, Germany*
[25]*Ludwig-Maximilians-Universität München, München, Germany*
[26]*Fachbereich Physik, University of Wuppertal, Wuppertal, Germany*
[27]*Panjab University, Chandigarh, India*
[28]*Delhi University, Delhi, India*
[29]*Tata Institute of Fundamental Research, Mumbai, India*
[30]*University College Dublin, Dublin, Ireland*
[31]*Korea Detector Laboratory, Korea University, Seoul, Korea*

[32] CINVESTAV, Mexico City, Mexico

[33] FOM-Institute NIKHEF and University of Amsterdam/NIKHEF, Amsterdam, The Netherlands

[34] Radboud University Nijmegen/NIKHEF, Nijmegen, The Netherlands

[35] Joint Institute for Nuclear Research, Dubna, Russia

[36] Institute for Theoretical and Experimental Physics, Moscow, Russia

[37] Moscow State University, Moscow, Russia

[38] Institute for High Energy Physics, Protvino, Russia

[39] Petersburg Nuclear Physics Institute, St. Petersburg, Russia

[40] Lund University, Lund, Sweden, Royal Institute of Technology and Stockholm University, Stockholm, Sweden, and Uppsala University, Uppsala, Sweden

[41] Lancaster University, Lancaster, United Kingdom

[42] Imperial College, London, United Kingdom

[43] University of Manchester, Manchester, United Kingdom

[44] University of Arizona, Tucson, Arizona 85721, USA

[45] Lawrence Berkeley National Laboratory and University of California, Berkeley, California 94720, USA

[46] California State University, Fresno, California 93740, USA

[47] University of California, Riverside, California 92521, USA

[48] Florida State University, Tallahassee, Florida 32306, USA

[49] Fermi National Accelerator Laboratory, Batavia, Illinois 60510, USA

[50] University of Illinois at Chicago, Chicago, Illinois 60607, USA

[51] Northern Illinois University, DeKalb, Illinois 60115, USA

[52] Northwestern University, Evanston, Illinois 60208, USA

[53] Indiana University, Bloomington, Indiana 47405, USA

[54] University of Notre Dame, Notre Dame, Indiana 46556, USA

[55] Iowa State University, Ames, Iowa 50011, USA

[56] University of Kansas, Lawrence, Kansas 66045, USA

[57] Kansas State University, Manhattan, Kansas 66506, USA

[58] Louisiana Tech University, Ruston, Louisiana 71272, USA

[59] University of Maryland, College Park, Maryland 20742, USA

[60] Boston University, Boston, Massachusetts 02215, USA

[61] Northeastern University, Boston, Massachusetts 02115, USA

[62] University of Michigan, Ann Arbor, Michigan 48109, USA

[63] Michigan State University, East Lansing, Michigan 48824, USA

[64] University of Mississippi, University, Mississippi 38677, USA

[65] University of Nebraska, Lincoln, Nebraska 68588, USA

[66] Princeton University, Princeton, New Jersey 08544, USA

[67] Columbia University, New York, New York 10027, USA

[68] University of Rochester, Rochester, New York 14627, USA

[69] State University of New York, Stony Brook, New York 11794, USA

[70] Brookhaven National Laboratory, Upton, New York 11973, USA

[71] Langston University, Langston, Oklahoma 73050, USA

[72] University of Oklahoma, Norman, Oklahoma 73019, USA

[73] Brown University, Providence, Rhode Island 02912, USA

[74] University of Texas, Arlington, Texas 76019, USA

[75] Southern Methodist University, Dallas, Texas 75275, USA

[76] Rice University, Houston, Texas 77005, USA

[77] University of Virginia, Charlottesville, Virginia 22901, USA

[78] University of Washington, Seattle, Washington 98195, USA

(Dated: February 7, 2008)

The $WW\gamma$ triple gauge boson coupling parameters are studied using $p\overline{p} \to \ell\nu\gamma + X\,(\ell = e, \mu)$ events at $\sqrt{s} = 1.96$ TeV. The data were collected with the DØ detector from an integrated luminosity of 162 pb$^{-1}$ delivered by the Fermilab Tevatron Collider. The cross section times branching fraction for $p\overline{p} \to W(\gamma) + X \to \ell\nu\gamma + X$ with $E_T^\gamma > 8$ GeV and $\Delta\mathcal{R}_{\ell\gamma} > 0.7$ is $14.8 \pm 1.6$(stat)$\pm 1.0$(syst) $\pm 1.0$(lum) pb. The one-dimensional 95% confidence level limits on anomalous couplings are $-0.88 < \Delta\kappa_\gamma < 0.96$ and $-0.20 < \lambda_\gamma < 0.20$.

The $W\gamma$ final states observed at hadron colliders provide an opportunity to study the self-interaction of electroweak bosons at the $WW\gamma$ vertex. The standard model (SM) description of electroweak physics is based on SU(2)$_L \otimes$U(1)$_Y$ gauge symmetry and specifies the $WW\gamma$ coupling. In the SM, production of a photon in associ-

ation with a $W$ boson occurs due to radiation of a photon from an incoming quark, from the $W$ boson due to direct $WW\gamma$ coupling, or from the outgoing $W$ boson decay lepton. To allow for non-SM couplings, a CP-conserving effective Lagrangian can be written with two coupling parameters: $\kappa_\gamma$ and $\lambda_\gamma$ [1, 2]. The SM predicts $\Delta\kappa_\gamma \equiv \kappa_\gamma - 1 = 0$ and $\lambda_\gamma = 0$. Non-standard couplings cause the effective Lagrangian to violate partial wave unitarity at high energies; it is necessary to introduce a form-factor with scale $\Lambda$ for each of the coupling parameters. The form-factors are introduced via the ansatz $\lambda \rightarrow \lambda/(1 + \hat{s}/\Lambda^2)^2$ with $\sqrt{\hat{s}}$ the $W\gamma$ invariant mass. In this analysis, the scale $\Lambda$ is set to 2 TeV. For sufficiently small values of $\Lambda$ the dependence on $\Lambda$ is relatively small. Deviations from the SM $WW\gamma$ couplings would cause an increase in the total $W\gamma$ production cross section and would enhance the production of photons with high transverse energy.

Limits on the $WW\gamma$ coupling parameters have been previously reported by the DØ [3] and CDF [4] collaborations using direct observation of $W\gamma$ final states in data collected from hadron collisions at the Fermilab Tevatron collider and by the UA2 [5] collaboration using the $Sp\overline{p}S$ collider at CERN. Searches for $W^+W^-$ final states at DØ [6] and CDF [7] have also been used to test $WW\gamma$ and $WWZ$ coupling parameters simultaneously. Similarly, experiments at the CERN LEP collider constrain the $WW\gamma$ and $WWZ$ coupling parameters simultaneously through observations of $W^+W^-$, single-$W$ boson, and single-$\gamma$ final states in electron-positron collisions [8]. Observation of $b \rightarrow s\gamma$ decays by the CLEO collaboration has also been used to constrain the coupling parameters [9].

The analyses discussed here use the DØ detector to observe $p\overline{p} \rightarrow \ell\nu\gamma + X (\ell = e$ or $\mu)$ events in collisions at $\sqrt{s} = 1.96$ TeV at the Fermilab Tevatron collider. The data samples used for the electron and muon channels correspond to integrated luminosities of 162 pb$^{-1}$ and 134 pb$^{-1}$, respectively. The DØ detector [10] features an inner tracker surrounded by a liquid-argon/uranium calorimeter and a muon spectrometer. The inner tracker consists of a silicon microstrip tracker (SMT) and a central fiber tracker (CFT), both located within a 2 T superconducting solenoidal magnet. The CFT covers $|\eta| \lesssim 1.8$ and the SMT covers $|\eta| \lesssim 3.0$ [11]. The calorimeter is longitudinally segmented into electromagnetic and hadronic layers and is housed in three cryostats: a central section covering $|\eta| \lesssim 1.1$ and two end-cap cryostats that extend coverage to $|\eta| \lesssim 4.0$. The muon detectors reside outside the calorimeter and consist of tracking detectors, scintillation counters, and a 1.8 T toroidal magnet. The muon detectors cover to $|\eta| \lesssim 2.0$. Luminosity is measured using scintillator arrays located in front of the end-cap cryostats and covering $2.7 \lesssim |\eta| \lesssim 4.4$.

Candidate events with electron decays of the $W$ boson ($W \rightarrow e\nu$) are collected using a suite of single electron triggers that require electromagnetic clusters in the calorimeter with at least 11 GeV of transverse energy ($E_T$). Offline electron identification requires the candidate electrons to be in the central calorimeter ($|\eta| < 1.1$), isolated in the calorimeter, have shower profiles consistent with those of electromagnetic objects, and have a track found in the tracking detectors matched to the calorimeter cluster. Similarly, photons are identified as central electromagnetic calorimeter clusters without a matched track that are isolated both in the calorimeter and in the tracking detectors. To suppress events with final state radiation of the photon from the outgoing lepton, and to avoid collinear singularities in calculations, the photon is required to be separated from the electron in $\eta - \phi$ space ($\Delta\mathcal{R} = \sqrt{(\eta_\gamma - \eta_\ell)^2 + (\phi_\gamma - \phi_\ell)^2} > 0.7$). Events used in this analysis are required to have $E_T^e > 25$ GeV, $E_T^\gamma > 8$ GeV, missing transverse energy using the full calorimeter $\not{E}_T > 25$ GeV, and $M_T > 40$ GeV/$c^2$, where $M_T$ is the transverse mass $\sqrt{2E_T^e \not{E}_T(1 - \cos\phi^{e\nu})}$ of the electron and $\not{E}_T$ vectors which are separated by $\phi^{e\nu}$ in azimuth.

Candidate events with muon decays of the $W$ boson ($W \rightarrow \mu\nu$) are collected using a suite of single muon triggers that require a high $p_T$ track in the muon detectors and a high $p_T$ track in the central tracking detectors. Offline muon identification additionally restricts muon candidates to the full central tracking acceptance ($|\eta| < 1.6$), requires matched central tracks, and imposes timing cuts to reduce backgrounds from cosmic and beam halo muons. Events with more than one identified muon are rejected to reduce backgrounds from $Z \rightarrow \mu\mu(\gamma)$. Events are required to have $p_T^\mu > 20$ GeV/$c$, $E_T^\gamma > 8$ GeV, $\not{E}_T > 20$ GeV, and there is no $M_T$ requirement for this analysis. Photon identification is the same for both electron and muon analyses.

The dominant background for both decay channels is $W$+jet production where a jet mimics a photon. The contribution of this background is estimated by using a large multijet data sample to measure the probability of jets to mimic photons. Some fraction of multijet events contains true photons, and this fraction has previously been seen to increase with increasing transverse energy as $1 - e^{a - bE_T}$ [12]. The systematic uncertainty on the probability of a jet being misidentified as a photon is taken to be the full difference between ignoring the presence of true photons in the multijet data sample and estimating their contribution with the above functional form. The method described above is dependent on agreement between the jet energy calibration and the electromagnetic energy calibration; as a check of the accuracy of the jet energy calibration, the method is repeated using jet-like objects that have a high fraction of calorimeter energy in the electromagnetic layers. This yields a background estimate consistent with the method based on jets.

A second class of background events comes from processes which produce an electron or muon, an electron

TABLE I: Summary of estimated backgrounds and numbers of events selected in each channel.

| | $e\nu\gamma$ Channel | $\mu\nu\gamma$ Channel |
|---|---|---|
| Luminosity | 162 pb$^{-1}$ | 134 pb$^{-1}$ |
| $W+$ jet background events | $58.7 \pm 4.5$ | $61.8 \pm 5.1$ |
| $\ell eX$ background events | $1.7 \pm 0.5$ | $0.7 \pm 0.2$ |
| $W\gamma \to \tau\nu\gamma$ background events | $0.42 \pm 0.02$ | $1.9 \pm 0.2$ |
| $Z\gamma \to \ell\ell\gamma$ background events | - | $6.9 \pm 0.7$ |
| Total background events | $60.8 \pm 4.5$ | $71.3 \pm 5.2$ |
| Selected events | 112 | 161 |
| Total signal events | $51.2 \pm 11.5$ | $89.7 \pm 13.7$ |

that is misidentified as a photon, and missing transverse energy. This background, labeled $\ell eX$, is small for the muon channel since very few processes produce a high $E_T$ muon and an electron. However, this background is significant for the electron channel since $Z(\to ee)+$jet (with a mismeasured jet leading to apparent missing transverse energy) processes have a relatively large cross section. To reduce this background, an additional criterion on the invariant mass of the electron and photon candidates is imposed, and events with $70 < M_{e\gamma} < 110$ GeV/$c^2$ are rejected. In both the electron and muon analyses, the $\ell eX$ background is estimated by reversing the track match requirement on the photon candidate (*i.e.* require a matched track) in $W\gamma$ candidate events. The number of $\ell eX$ events in which the electron is isolated and does not have a matched track (and therefore is misidentified as a photon) is then estimated using the known track matching and track isolation inefficiencies.

Small backgrounds from $Z\gamma$, where one lepton from the $Z$ decay is not reconstructed, and $W \to \tau\nu\gamma$, where the $\tau$ decays into an electron or muon, are estimated from Monte Carlo samples. The background estimates and numbers of events observed in the data are summarized in Table I.

The efficiencies of the triggers and the lepton identification cuts are measured using $Z \to ee, \mu\mu$ events. Efficiencies for electrons are $0.96 \pm 0.02$ for the trigger, $0.84 \pm 0.01$ for the calorimeter identification requirements, and $0.78 \pm 0.01$ for the track match requirement. For muons, the trigger efficiency is $0.74 \pm 0.01$, the offline reconstruction efficiency is $0.77 \pm 0.02$, and the efficiency of the track match requirement is $0.98 \pm 0.01$. The efficiency of the requirement of no more than one muon in muon candidate events is estimated to be $0.942 \pm 0.004$ by counting the fraction of $Z \to ee$ events containing a muon. The track isolation efficiency used for the $\ell eX$ background estimation is measured using $Z \to ee$ events and is $0.95 \pm 0.01$. The efficiency of the calorimeter requirements in photon identification is estimated using a full GEANT3 simulation of the detector [13]. The probability for unrelated tracks to overlap with the photon and cause it to fail the track isolation requirements is mea-

sured using $Z \to ee$ events by measuring the probability of an electron to have nearby tracks after the event is rotated in $\phi$ by ninety degrees. The overall efficiency for photon identification is $0.81 \pm 0.01$. The total efficiencies are $0.51 \pm 0.02$ for the electron channel and $0.43 \pm 0.01$ for the muon channel.

The acceptances due to the kinematic and geometric requirements in the analyses are calculated using a Monte Carlo generator [2] that fully models $W\gamma$ production to leading order in quantum chromodynamics (QCD) and electroweak couplings and allows anomalous coupling values to be set. The detector response is simulated using a parameterized detector simulation. The effects of higher order QCD processes are accounted for by the introduction of a $K$-factor of 1.335 [2], and the transverse momentum spectrum of the $W$ boson is simulated using parton showers in PYTHIA [14]. The detector acceptance calculation has a very small dependence on the simulation of the transverse momentum of the $W$ boson. The CTEQ6L parton distribution function (PDF) [15] is used for the proton and anti-proton. The acceptances are $0.045 \pm 0.002$ for the electron channel and $0.102 \pm 0.003$ for the muon channel with the uncertainties dominated by the PDF uncertainty.

The measured cross sections times branching fractions $\sigma(p\bar{p} \to W(\gamma) + X \to \ell\nu\gamma + X)$ with $E_T^\gamma > 8$ GeV and $\Delta\mathcal{R}_{\ell\gamma} > 0.7$ are $13.9 \pm 2.9(\text{stat}) \pm 1.6(\text{syst}) \pm 0.9(\text{lum})$ pb for the electron channel and $15.2 \pm 2.0(\text{stat}) \pm 1.1(\text{syst}) \pm 1.0(\text{lum})$ pb for the muon channel. The three components of the cross section uncertainty are: statistics; systematic effects associated with the background subtraction, acceptance calculation, and object identification; and the systematic uncertainties in the luminosity measurement. Combining events from the two decay channels and accounting for correlations in the systematic uncertainties yields a combined cross section times branching fraction of $14.8 \pm 1.6(\text{stat}) \pm 1.0(\text{syst}) \pm 1.0(\text{lum})$ pb. The SM prediction calculated by the Monte Carlo generator using the $K$-factor and the CTEQ6L PDF is $16.0 \pm 0.4$ pb, where the uncertainty is due to PDF uncertainty. The prediction is in agreement with the measurements.

The photon $E_T$ spectrum of the candidate events is shown with the background estimation and the SM expectation in Fig. 1. The distribution is described well by the SM, and no enhancement of the photon $E_T$ spectrum is seen at high transverse energy. Limits on anomalous couplings are determined by performing a binned likelihood fit to the photon $E_T$ spectrum. The effect of anomalous couplings is more pronounced at high $W\gamma$ transverse mass, $M_T(W,\gamma)$, so only events with $M_T(W,\gamma) > 90$ GeV/$c^2$ are used for the distributions in the likelihood fit. The $M_T(W,\gamma)$ distribution before this requirement is shown in Fig. 2. Monte Carlo distributions of the photon $E_T$ spectrum are generated with a range of anomalous coupling values, and the likelihood of the data distri-
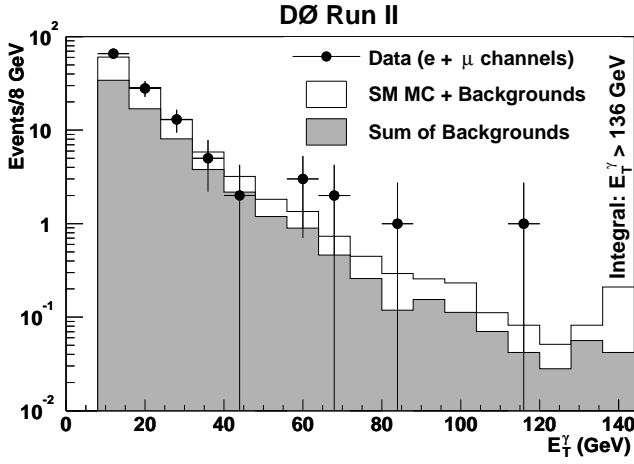
FIG. 1: The photon $E_T$ spectrum for the $W\gamma$ candidates with $M_T(W,\gamma) > 90$ GeV/$c^2$. The points with error bars are the data. The open histogram is the sum of the SM Monte Carlo prediction and the background estimate. The background estimate is shown as the shaded histogram. The right-most bin shows the sum of all events with photon $E_T$ above 136 GeV.
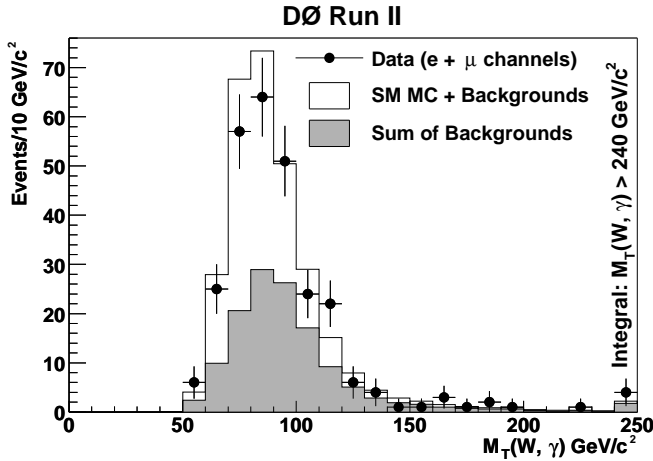


FIG. 2: The $M_T(W,\gamma)$ spectrum for the $W\gamma$ candidates. The points with error bars are the data. The open histogram is the sum of the SM Monte Carlo prediction and the background estimate. The background estimate is shown as the shaded histogram. The right-most bin shows the sum of all events with $M_T(W,\gamma)$ above 240 GeV.

bution being consistent with the generated distribution is calculated. The uncertainties in the background estimates, efficiencies, acceptances, and the luminosity are included in the likelihood calculation using Gaussian distributions.

The limits on the $WW\gamma$ coupling parameters are shown in Fig. 3, with the contour showing the two-dimensional 95% confidence level (CL) exclusion limits for the coupling parameters, the point representing the Standard Model value and the error bars showing the
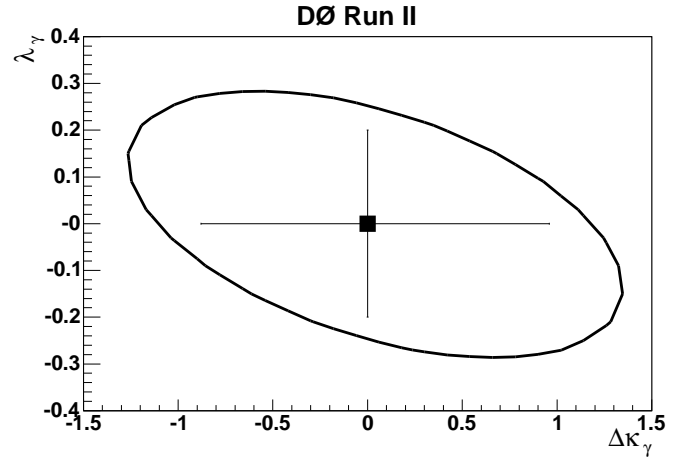


FIG. 3: Limits on the $WW\gamma$ coupling parameters $\Delta\kappa_\gamma$ and $\lambda_\gamma$. The point indicates the SM value with the error bars showing the 95% CL intervals in one dimension. The ellipse represents the two-dimensional 95% CL exclusion contour.

one-dimensional 95% CL intervals. The one-dimensional exclusion limits on each parameter are $-0.88 < \Delta\kappa_\gamma < 0.96$ and $-0.20 < \lambda_\gamma < 0.20$, where the limit on $\Delta\kappa_\gamma$ assumes $\lambda_\gamma$ is fixed to the SM value and vice versa and $\Lambda = 2$ TeV.

In summary, the cross section times branching fraction for the process $p\overline{p} \rightarrow W(\gamma) + X \rightarrow \ell\nu\gamma + X$ with $E_T^\gamma > 8$ GeV and $\Delta\mathcal{R}_{\ell\gamma} > 0.7$ is measured to be $14.8 \pm 1.6(\text{stat})\pm 1.0(\text{sys})\pm 1.0(\text{lum})$ pb using the DØ detector during Run II of the Tevatron. The measured cross section is in agreement with the SM expectation of $16.0 \pm 0.4$ pb. Limits at the 95% confidence level on anomalous $WW\gamma$ couplings are extracted using the photon transverse energy spectrum and are $-0.88 < \Delta\kappa_\gamma < 0.96$ and $-0.20 < \lambda_\gamma < 0.20$. These limits represent the most stringent constraints on anomalous $WW\gamma$ couplings obtained by direct observation of $W\gamma$ production.

[*] Visitor from University of Zurich, Zurich, Switzerland.

[1] K. Hagiwara *et al.*, Nucl. Phys. **B282**, 253 (1987).

[2] U. Baur and E. L. Berger, Phys. Rev. D **41**, 1476 (1990).

[3] DØ Collaboration, S. Abachi *et al.*, Phys. Rev. Lett. **78**, 3634 (1997).

[4] CDF Collaboration, F. Abe *et al.*, Phys. Rev. Lett. **75**, 1017 (1995); CDF Collaboration, D. Acosta *et al.*, Phys. Rev. Lett. **94**, 041803 (2005).

[5] UA2 Collaboration, J. Alitti *et al.*, Phys. Lett. B **277**, 194 (1992).

[6] DØ Collaboration, B. Abbott *et al.*, Phys. Rev. D **60**, 082002 (1999); DØ Collaboration, B. Abbott *et al.*, Phys. Rev. D **58**, Rapid Communications 051101 (1998).

[7] CDF Collaboration, F. Abe *et al.*, Phys. Rev. Lett. **75**, 1017 (1995); CDF Collaboration, F. Abe *et al.*, Phys. Rev. Lett. **78**, 4536 (1997).

[8] LEP Electroweak Working Group, D. Abbaneo *et al.*, CERN-PH-EP/2004-069, hep-ex/0412015.

[9] CLEO Collaboration, M. S. Alam *et al.*, Phys. Rev. Lett. **74**, 2885 (1995).

[10] DØ Collaboration, V. Abazov *et al.*, in preparation for submission to Nucl. Instrum. Methods Phys. Res. A;T. LeCompte and H. T. Diehl, Ann. Rev. Nucl. Part. Sci. **50**, 71 (2000).

[11] The DØ coordinate system is cylindrical with the $z$-axis along the beamline and the polar and azimuthal angles denoted as $\theta$ and $\phi$ respectively. The pseudorapidity is defined as $\eta = -\ln\tan(\theta/2)$.

[12] DØ Collaboration, S. Abachi *et al.*, Phys. Rev. Lett. **77**, 5011 (1996).

[13] R. Brun *et al.*, CERN-DD-78-2-REV.

[14] T. Sjöstrand *et. al.*, Comp. Phys. Commun. **135**, 238 (2001).

[15] CTEQ Collaboration, J. Pumplin *et al.*, JHEP **0207**, 012 (2002); CTEQ Collaboration, D. Stump *et al.*, JHEP **0310**, 046 (2003).